BLACK HOLES

# Cygnus X-1 contains a 21–solar mass black hole—Implications for massive star winds

James C. A. Miller-Jones[1]*, Arash Bahramian[1], Jerome A. Orosz[2], Ilya Mandel[3,4,5], Lijun Gou[6,7], Thomas J. Maccarone[8], Coenraad J. Neijssel[3,4,5], Xueshan Zhao[6,7], Janusz Ziółkowski[9], Mark J. Reid[10], Phil Uttley[11], Xueying Zheng[6,7]†, Do-Young Byun[12,13], Richard Dodson[14], Victoria Grinberg[15], Taehyun Jung[12,13], Jeong-Sook Kim[12], Benito Marcote[16], Sera Markoff[11,17], María J. Rioja[14,18,19], Anthony P. Rushton[20,21], David M. Russell[22], Gregory R. Sivakoff[23], Alexandra J. Tetarenko[24], Valeriu Tudose[25], Joern Wilms[26]

The evolution of massive stars is influenced by the mass lost to stellar winds over their lifetimes. These winds limit the masses of the stellar remnants (such as black holes) that the stars ultimately produce. We used radio astrometry to refine the distance to the black hole x-ray binary Cygnus X-1, which we found to be $2.22^{+0.18}_{-0.17}$ kiloparsecs. When combined with archival optical data, this implies a black hole mass of 21.2 ± 2.2 solar masses, which is higher than previous measurements. The formation of such a high-mass black hole in a high-metallicity system (within the Milky Way) constrains wind mass loss from massive stars.

Gravitational wave detections of black hole merger events have revealed a population of black holes with masses ranging from 7 to 50 solar masses ($M_\odot$) (*1*). Black holes that interact with a companion star are visible to electromagnetic observations as an x-ray binary. Radial velocity measurements of these companion stars have shown that black holes in x-ray binaries all have masses below 20 $M_\odot$ (*2*). The highest measured black hole mass in an x-ray binary is 15.65 ± 1.45 $M_\odot$ for the extragalactic system M33 X-7 (*3*).

The mass of a black hole is initially set by the properties of its progenitor star then can increase through accretion or mergers over its lifetime. The relevant properties of the progenitor include its initial mass and abundance of elements heavier than helium (its metallicity), the mass lost in stellar winds over its lifetime, and the evolutionary pathway that it followed, which can be strongly influenced by a binary companion. Mass measurements for massive stellar-mass black holes constrain stellar and binary evolution models (*4*) and predictions of the expected black hole merger rates.

The x-ray binary Cygnus X-1 (V1357 Cyg) (coordinates are provided in table S1) contains a black hole in a 5.6-day orbit with a more massive supergiant donor star, of spectral type O. Previous estimates of its component masses were based on a parallax measurement, in which the apparent annual angular shift in the source position relative to more distant objects was measured by using radio very-long-baseline interferometry. With trigonometry, this gave a distance of $1.86^{+0.12}_{-0.11}$ kpc (*5*). When combined with optical radial velocity measurements of the system, these data yielded a black hole mass of 14.8 ± 1.0 $M_\odot$ (*6*). However, the derived system parameters are then inconsistent with the expected mass-luminosity relation for the donor, if it is a hydrogen-burning main sequence star (*7*). The optical parallax measurement of 0.42 ± 0.03 milli–arc sec measured with the *Gaia* space telescope (*8*), after correction for a known zero-point offset of ≈0.05 milli–arc sec [with estimates ranging from 0.03 to 0.08 milli–arc sec (*9*)], becomes 0.47 ± 0.04 milli–arc sec. This is inconsistent with the radio value of 0.54 ± 0.03 milli–arc sec (*5*) and is unlikely to be due to orbital displacement of the donor star because the *Gaia* value is the average over 119 orbital periods.

Between 29 May 2016 and 3 June 2016, we performed six observations (one per day) of Cygnus X-1 with the Very Long Baseline Array (VLBA) at 8.4 GHz, sampling one full orbital period. To reduce systematic uncertainties in our position measurements, we phase referenced the data to a nearby calibrator source 0.4° from Cygnus X-1 (*10*). These data resolve the orbital motion of the black hole as projected onto the downstream surface from which the jet emission can escape, which is called the photosphere. We found that the orbit is clockwise on the plane of the sky (Fig. 1), which is in agreement with previous observations (*5*).

Combining the orbital phase coverage of our VLBA data with archival observations (*5*), we simultaneously fitted the entire data set (covering a 7.4-year baseline) with a full astrometric solution that incorporated linear motion across the sky (proper motion), parallax, and orbital motion. Fitting both the right ascension and declination coordinates showed an orbital phase dependence in the direction of the residuals. We attribute this to the effect of free-free absorption in the stellar wind, which is known to modulate the radio emission of Cygnus X-1 on the orbital period (*11*). Electrons in the ionized wind of the O star can absorb radio photons in the presence of atomic nuclei, preventing the radio emission from the inner parts of the jet from reaching us. This free-free absorption is reduced as the stellar wind density decreases, as it moves away from the O star, allowing radiation to escape from further downstream. As the black hole (from which the jet is launched) moves around its orbit, the varying path length through the stellar wind imprints an orbital periodicity on the apparent radio position along the jet axis. When the black hole is on the far side of the donor star, the path length and hence absorption are maximized, pushing the radio photosphere downstream along the jet axis (*10*).

To negate the effect of the stellar wind absorption, we therefore repeated our astrometric model fitting in one dimension only, perpendicular to the known jet axis. This removed the orbital phase dependence of the fit residuals perpendicular to the jet axis (Fig. 2). Our measured semimajor axis of the black hole orbit is 58 ± 20 micro–arc sec, and our revised parallax measurement is 0.46 ± 0.04 milli–arc sec, which is consistent with the optical value from *Gaia* after correction for the zero point. After converting our measured



[1]International Centre for Radio Astronomy Research–Curtin University, Perth, WA 6845, Australia. [2]Astronomy Department, San Diego State University, San Diego, CA 92182-1221, USA. [3]School of Physics and Astronomy, Monash University, Clayton, VIC 3800, Australia. [4]OzGrav: The Australian Research Council Centre of Excellence for Gravitational Wave Discovery, Hawthorn, VIC 3122, Australia. [5]School of Physics and Astronomy, University of Birmingham, Edgbaston, Birmingham B15 2TT, UK. [6]Key Laboratory for Computational Astrophysics, National Astronomical Observatories, Chinese Academy of Sciences, Beijing 100012, China. [7]University of Chinese Academy of Sciences, Beijing 100012, China. [8]Department of Physics and Astronomy, Texas Tech University, Lubbock, TX 79409-1051, USA. [9]Nicolaus Copernicus Astronomical Center, PL-00-716 Warsaw, Poland. [10]Center for Astrophysics, Harvard and Smithsonian, Cambridge, MA 02138, USA. [11]Anton Pannekoek Institute for Astronomy, University of Amsterdam, 1098 XH Amsterdam, Netherlands. [12]Korea Astronomy and Space Science Institute, Daejeon 34055, Republic of Korea. [13]University of Science and Technology, Daejeon 34113, Republic of Korea. [14]International Centre for Radio Astronomy Research–University of Western Australia, Crawley, WA 6009, Australia. [15]Institut für Astronomie und Astrophysik, Universität Tübingen, 72076 Tübingen, Germany. [16]Joint Institute for Very Long Baseline Interferometry European Research Infrastructure Consortium, 7991 PD Dwingeloo, Netherlands. [17]Gravitation and Astroparticle Physics Amsterdam Institute, University of Amsterdam, NL-1098 XH Amsterdam, Netherlands. [18]Commonwealth Scientific and Industrial Research Organisation, Astronomy and Space Science, Perth, WA 6102, Australia. [19]Observatorio Astronómico Nacional, Instituto Geográfico Nacional, 28014 Madrid, Spain. [20]Department of Physics, Astrophysics, University of Oxford, Oxford OX1 3RH, UK. [21]School of Physics and Astronomy, University of Southampton, Southampton SO17 1BJ, UK. [22]Center for Astro, Particle, and Planetary Physics, New York University Abu Dhabi, Abu Dhabi, United Arab Emirates. [23]Department of Physics, Centennial Centre for Interdisciplinary Science, University of Alberta, Edmonton, AB T6G 2E1, Canada. [24]East Asian Observatory, Hilo, HI 96720, USA. [25]Institute for Space Sciences, 077125 Bucharest-Magurele, Romania. [26]Dr. Karl Remeis-Sternwarte and Erlangen Centre for Astroparticle Physics, Friedrich-Alexander-Universität Erlangen-Nürnberg, 96049 Bamberg, Germany.
***Corresponding author. Email: james.miller-jones@curtin.edu.au.** †Present address: Max-Planck-Institut für Extraterrestrische Physik, D-85748 Garching, Germany.

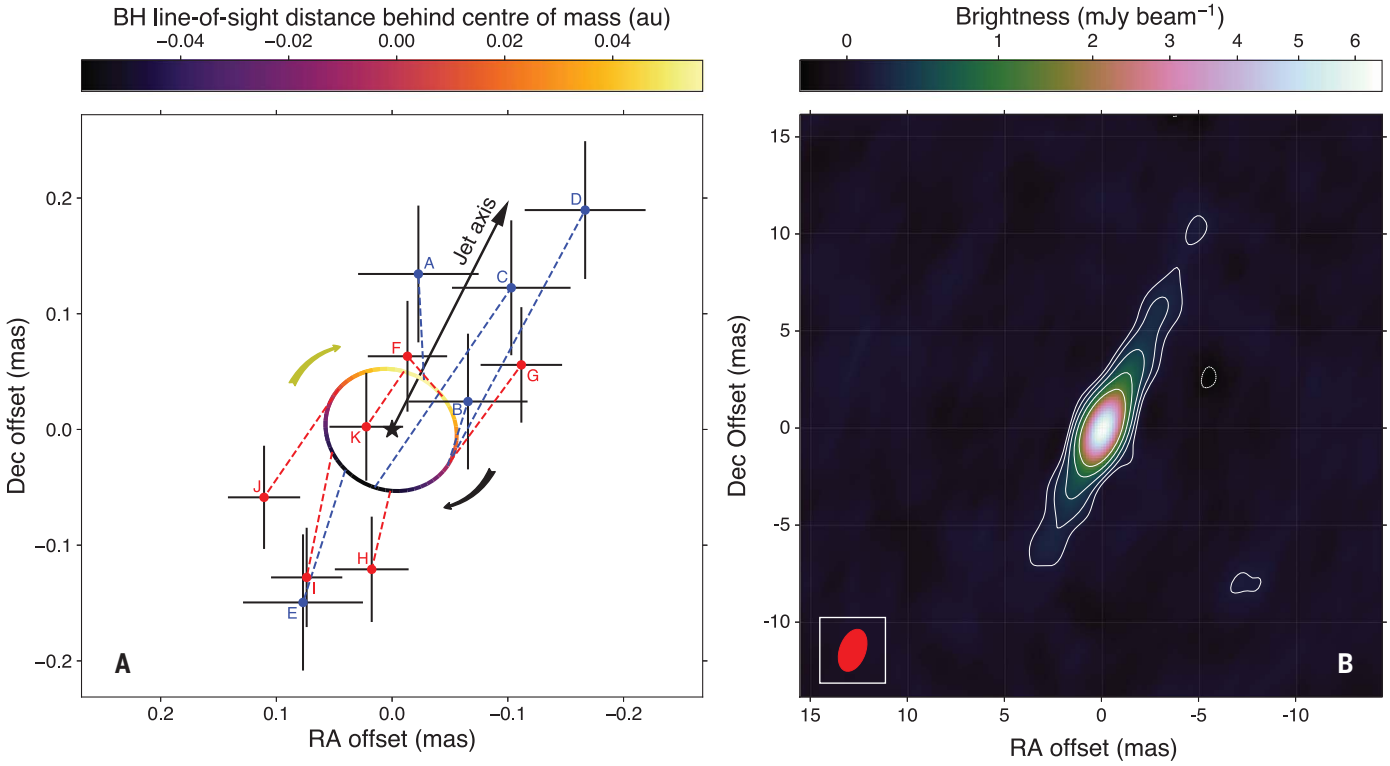


**Fig. 1. Cygnus X-1 and its best fitting model orbit on the plane of the sky.** (**A**) Astrometric measurements from the new (red points) and archival (blue points) VLBA data (*5*). Error bars show the 68% confidence level. The letter labels indicate the chronological ordering of the observations, as detailed in table S1. Dashed lines link the measured positions to the location on the fitted orbit, shown as the colored ellipse. The color bar indicates the location of the black hole along the line of sight, relative to the center of mass of the system (shown as the black star), with positive values being behind the center of mass. Arrows indicate the direction of orbital motion and the jet axis. (**B**) Stacked radio image of the jet in color, with white contours every $\pm(\sqrt{2})$ times the root mean square noise level of 23 microjanskys (μJy) per beam. The red ellipse indicates the size and shape of the synthesized beam. Although the measured positions scatter along the jet axis, the motion perpendicular to the jet axis is reproduced by the astrometric model (Fig. 2). Coordinates are given in right ascension (RA) and declination (Dec), J2000 equinox. mas, milli–arc seconds.

parallax to a distance by using an exponentially decreasing space density prior (*12*), we found a distance of $2.22^{+0.18}_{-0.17}$ kpc.

This revised distance affects the system parameters derived from optical modeling (*6*). We reanalyzed the optical light curve (*13*) and radial velocity curves (*14*), adopting our revised distance and additional constraints on the effective temperature, surface gravity, and helium abundance of the donor star (*15*). We found substantially higher masses for both the black hole ($21.2 \pm 2.2\ M_\odot$) (fig. S8) and the donor star ($40.6^{+7.7}_{-7.1}\ M_\odot$). The black hole orbital semimajor axis derived from this reanalysis of the optical data are 0.160 ± 0.013 astronomical units (au) (Table 1), which equates to 73 ± 8 micro–arc sec at our best-fitting distance of $2.22^{+0.18}_{-0.17}$ kpc. This is consistent with the value derived directly from our VLBA astrometry (Fig. 2 and table S3).

The higher donor mass and greater luminosity inferred from the larger distance (Table 1) bring the system into closer agreement with the mass-luminosity relationship for main-sequence hydrogen-burning stars of solar composition (*7*, *10*). However, the measured surface composition shows that the helium-to-hydrogen ratio is enhanced by a factor of 2.6 relative to the solar composition (*15*). This would imply a slightly different mass-luminosity relationship if the surface abundance is indicative of the overall composition of the donor star but remains broadly consistent with our revised values (Fig. 3).

The higher mass and distance could also affect the black hole spin determined from spectral fitting of the x-ray continuum (*16*). We therefore reanalyzed archival x-ray data using a continuum-fitting method, assuming the black hole spin axis is aligned with the orbital plane. We found the black hole dimensionless spin parameter $a_* > 0.9985$, which is close to the maximum possible value of 1, although this could be affected by systematic uncertainties (*10*). Even if the true value is less extreme, it would still be very high, which is consistent with previous results derived from both the continuum and iron line-fitting methods (*16*, *17*). Although the spin derived from our analysis would be reduced if the black hole spin axis were not aligned with the orbital plane, even a 15° misalignment would still require a high spin, $a_* = 0.9696$.

As an x-ray binary system with a high-mass donor star, the black hole in Cygnus X-1 cannot have been spun up by accretion from its companion at the maximum theoretical rate (known as the Eddington limit; ~$2 \times 10^{-7}\ M_\odot$ year$^{-1}$ for Cygnus X-1) because that cannot occur for longer than the lifetime of the donor [~4 million years for our inferred mass (*18*)]. The accretion time may be close to the age of the jet-inflated nebula surrounding the source [a few tens of thousands of years (*19*)]. The current spin must therefore reflect the angular momentum of the core of the progenitor star. An evolutionary pathway that could explain this is main sequence mass transfer from the black hole progenitor to the secondary star [case A mass transfer (*20*)] with the core of the progenitor tidally locked and hence rapidly rotating, which can produce high black hole spins (*21*). This evolutionary pathway for Cygnus X-1 would imply a spin axis of the black hole progenitor that is aligned with the orbital angular momentum. Given the very low velocity kick of $9 \pm 2$ km s$^{-1}$ imparted to the system upon black hole formation [as determined with VLBA astrometry (*22*)], the

**Table 1. Fitted and derived physical parameters for Cygnus X-1.** The inclination $i$, eccentricity $e$, and argument of periastron $\omega$ of the orbit; the mass $M_1$, Roche-lobe filling factor $f_1$, effective temperature $T_{eff}$, and semi-amplitude of the radial velocity curve $K_1$ for the O-star; a phase shift parameter $\phi$ to account for ephemeris errors; and the ratio $\Omega_{rot}$ of the rotational frequency of the O-star to the orbital frequency (the top nine parameters) were directly fitted in the model. The black hole mass $M_{BH}$; the radius $R_1$ in solar radii $R_\odot$, luminosity $L$ in solar luminosities $L_\odot$, and surface gravity $g_1$ of the O-star; and the semimajor axes of the full orbit $a$, stellar orbit $a_1$, and black hole orbit $a_{BH}$ (the bottom seven parameters) were derived from the fitted parameters, by using the known orbital period (*13*). Lower and upper bounds encompass the 68% confidence interval.

| Parameter | Median | Mode | Lower bound | Upper bound |
|---|---|---|---|---|
| $i$ (deg) | 27.51 | 27.33 | 26.94 | 28.28 |
| $e$ | 0.0189 | 0.0186 | 0.0163 | 0.0217 |
| $\omega$ (deg) | 306.6 | 306.3 | 300.3 | 313.1 |
| $M_1$ ($M_\odot$) | 40.6 | 39.8 | 33.5 | 48.3 |
| $f_1$ | 0.960 | 0.999 | 0.930 | 0.988 |
| $T_{eff}$ (K) | 31,138 | 31,158 | 30,398 | 31,840 |
| $K_1$ (km s$^{-1}$) | 75.21 | 75.18 | 74.80 | 75.63 |
| $\phi$ | 0.0024 | 0.0023 | 0.0013 | 0.0034 |
| $\Omega_{rot}$ | 1.05 | 1.04 | 0.95 | 1.16 |
| $M_{BH}$ ($M_\odot$) | 21.2 | 21.4 | 18.9 | 23.4 |
| $R_1$ ($R_\odot$) | 22.3 | 22.2 | 20.6 | 24.1 |
| log($L/L_\odot$) | 5.625 | 5.606 | 5.547 | 5.698 |
| log($g_1$/cm s$^{-2}$) | 3.348 | 3.351 | 3.335 | 3.360 |
| $a$ (au) | 0.244 | 0.243 | 0.231 | 0.256 |
| $a_1$ (au) | 0.0838 | 0.0840 | 0.0816 | 0.0856 |
| $a_{BH}$ (au) | 0.160 | 0.159 | 0.147 | 0.173 |

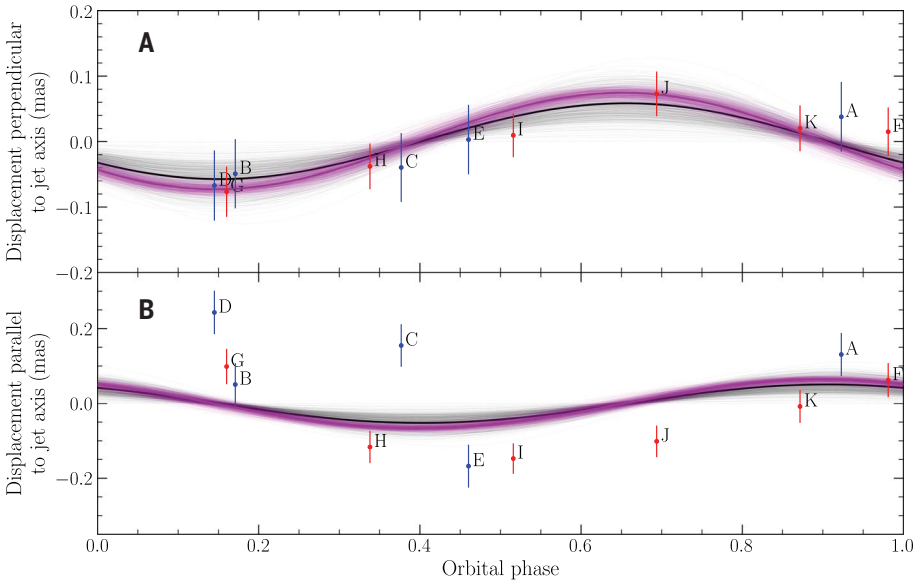


**Fig. 2. Orbital displacements relative to the best-fitting one-dimensional astrometric model.** Parallax and proper motion signatures have been subtracted. (**A**) The measured displacements perpendicular to the jet axis. Red points are our VLBA data, and blue points are the archival observations (*5*), with error bars showing the 68% confidence level. Labels reflect the chronological ordering of the observations, as listed in table S1. Black and magenta lines show 500 random draws from the posterior probability distribution of the orbital parameters for radio and optical models, respectively (with the posterior medians indicated with thicker lines), which are consistent within the uncertainties. The data were only fitted perpendicular to the jet axis. (**B**) The measured displacements parallel to the jet axis show that the measured core positions are primarily downstream of the model predictions when the black hole is close to superior conjunction (behind the donor star; phases close to 0.0) and upstream when the black hole is close to inferior conjunction (phases close to 0.5), as expected for wind absorption.

black hole spin should still be aligned with the orbital inclination, as we assumed above. This scenario is also consistent with the low orbital eccentricity (*6*) and the lack of strong quasi-periodic variability seen in the x-ray power density spectra of the source (*23*).

This evolutionary pathway is associated with enhanced nitrogen abundances, as observed in the donor spectrum (*21*). The transfer of enriched material from the black hole progenitor could also explain the high helium abundance in the spectrum of the donor star (*15*). In the absence of convection, which is expected to be limited to a very thin surface layer in the envelope of a 40 $M_\odot$ star of solar [or possibly supersolar (*15*)] metallicity, some fraction of this material would be retained on the surface for up to ~$10^5$ years (supplementary text). As a surface contaminant, this would not be reflective of the overall composition of the donor. Our revised values for the mass and luminosity of the donor star are consistent with theoretical expectations (Fig. 3) (*10*).

The increase in the inferred black hole mass makes Cygnus X-1 more massive than previously observed black holes in x-ray binaries (*24*), surpassing M33 X-7. M33 X-7 has a substantially subsolar metallicity (~0.1 times the solar metallicity, $Z_\odot$) (*3*). However, the metallicity of the mass donor in Cygnus X-1 is much higher. It has been estimated to be approximately twice solar (*15*), although the complexity of the system makes precise measurements challenging, and the true value may be closer to solar (*10*). The existence of a 21 $M_\odot$ black hole at solar (or supersolar) metallicity implies that mass loss rate prescriptions (*4*) overestimate the mass loss during the luminous blue variable or Wolf-Rayet stages of stellar evolution (*25*, *26*). Assuming solar metallicity for the system, we found that either the mass loss rates in Wolf-Rayet winds from naked helium stars are reduced by a factor of three compared with those of current models (*4*), or those in luminous blue variable winds are reduced by at least a third, or both (supplementary text).

Reduced mass loss can lead to higher progenitor masses at the time of the supernova. It may also allow massive stars at moderate metallicities to retain hydrogen as they evolve [although probably not in the evolutionary history of Cygnus X-1, in which the black hole's progenitor likely had most of its hydrogen stripped off by the companion while the former was still on the main sequence (supplementary text)]. This would change the observational signatures of supernovae—for example, producing hydrogen-rich (pulsational) pair-instability supernovae (*27*). Enrichment of the interstellar medium by stellar winds could be reduced, and depending on which phases of the stellar evolution are most affected by reduced winds, the contribution of

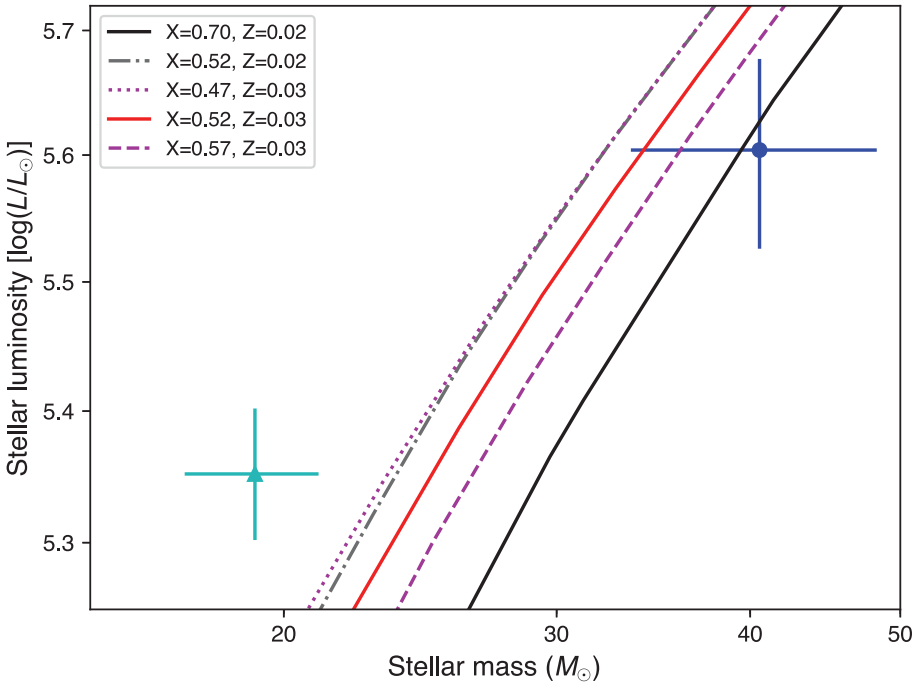


**Fig. 3. Predicted mass-luminosity relations for high-mass main sequence stars.** Masses are given in solar masses, and luminosities are relative to the solar luminosity $L_{\odot}$. The black solid line shows the predicted relation for a standard composition [hydrogen mass fraction $X$ = 0.70; mass fraction of heavy elements $Z$ = 0.02 (*10*)]. The gray dot-dashed line is for an enhanced helium abundance, $X$ = 0.52, $Z$ = 0.02 [as inferred for the surface abundance of the donor star (*15*)]. The red solid line shows the effect of an increased metallicity, with $Z$ = 0.03, $X$ = 0.52. The magenta dotted line and dashed line show the effect of the uncertainty on the helium abundance (*15*). The mass and luminosity determined from previous observations (*6*) are shown as the cyan triangle. The values derived from our observations are shown as the blue circle, which lies closer to the theoretical relations, irrespective of composition or metallicity. Error bars show 68% confidence levels.

massive stars to the reionization of the Universe may be affected (supplementary text).

The black hole mass distribution inferred from gravitational wave events favors larger masses than predicted by stellar and binary evolution models. Variations in metallicity-specific star formation history that favor greater star formation at lower metallicity have been proposed as an explanation (*28*, *29*). Reduced stellar winds would increase the mass of black holes that could be produced at all metallicities, so that massive gravitational wave sources could form at intermediate (not just very low) metallicities. This would imply that the progenitors of some gravitational wave events could have formed at a correspondingly lower redshift, with a shorter delay time between binary formation and merger.

The high spin of Cygnus X-1 [in common with most high-mass black hole x-ray binaries, which appear to be predominantly rapidly spinning (*30*)] implies that it followed an evolutionary pathway different to that of the majority of black holes detected in gravitational wave events, which have spins that are either low or misaligned (*31*). Given the current orbital separation, we do not expect Cygnus X-1 to undergo a binary black hole merger in a time scale equal to the age of the Universe.

## REFERENCES AND NOTES


1. B. P. Abbott *et al*, *Astrophys. J.* **882**, L24 (2019).
2. J. Casares, P. G. Jonker, *Space Sci. Rev.* **183**, 223–252 (2014).
3. J. A. Orosz *et al*., *Nature* **449**, 872–875 (2007).
4. K. Belczynski *et al*., *Astrophys. J.* **714**, 1217–1226 (2010).
5. M. J. Reid *et al*., *Astrophys. J.* **742**, 83 (2011).
6. J. A. Orosz *et al*., *Astrophys. J.* **742**, 84 (2011).
7. J. Ziółkowski, *Mon. Not. R. Astron. Soc. Lett.* **440**, L61–L65 (2014).
8. Gaia Collaboration *et al*., *Astron. Astrophys.* **616**, A1 (2018).
9. V. C. Chan, J. Bovy, *Mon. Not. R. Astron. Soc.* **493**, 4367–4381 (2020).
10. Materials and methods are available as supplementary materials.
11. C. Brocksopp, R. P. Fender, G. G. Pooley, *Mon. Not. R. Astron. Soc.* **336**, 699–704 (2002).
12. T. L. Astraatmadja, C. A. L. Bailer-Jones, *Astrophys. J.* **832**, 137 (2016).
13. C. Brocksopp, A. E. Tarasov, V. M. Lyuty, P. Roche, *Astron. Astrophys.* **343**, 861 (1999).
14. D. R. Gies *et al*., *Astrophys. J.* **583**, 424–436 (2003).
15. V. V. Shimanskii *et al*., *Astron. Rep.* **56**, 741–760 (2012).
16. L. Gou *et al*., *Astrophys. J.* **742**, 85 (2011).
17. R. Duro *et al*., *Astron. Astrophys.* **589**, A14 (2016).
18. A. Bressan *et al*., *Mon. Not. R. Astron. Soc.* **427**, 127–145 (2012).
19. D. M. Russell, R. P. Fender, E. Gallo, C. R. Kaiser, *Mon. Not. R. Astron. Soc.* **376**, 1341–1349 (2007).
20. R. Kippenhahn, A. Weigert, *Z. Astrophys.* **65**, 251 (1967).
21. Y. Qin, P. Marchant, T. Fragos, G. Meynet, V. Kalogera, *Astrophys. J.* **870**, L18 (2019).
22. I. F. Mirabel, I. Rodrigues, *Science* **300**, 1119–1120 (2003).
23. V. Grinberg *et al*., *Astron. Astrophys.* **565**, A1 (2014).
24. B. E. Tetarenko, G. R. Sivakoff, C. O. Heinke, J. C. Gladstone, *Astrophys. J.* **222**, 15 (2016).
25. J. R. Hurley, O. R. Pols, C. A. Tout, *Mon. Not. R. Astron. Soc.* **315**, 543–569 (2000).
26. J. S. Vink, A. de Koter, H. J. G. L. M. Lamers, *Astron. Astrophys.* **369**, 574–588 (2001).
27. I. Arcavi *et al*., *Nature* **551**, 210–213 (2017).
28. C. J. Neijssel *et al*., *Mon. Not. R. Astron. Soc.* **490**, 3740–3759 (2019).
29. M. Chruslinska, G. Nelemans, *Mon. Not. R. Astron. Soc.* **488**, 5300–5326 (2019).
30. M. C. Miller, J. M. Miller, *Phys. Rep.* **548**, 1–34 (2015).
31. W. M. Farr *et al*., *Nature* **548**, 426–429 (2017).
32. J. C. A. Miller-Jones *et al*., Cygnus X-1: Emerging view of a 21-solar mass black hole in the Milky Way. Zenodo (2021); doi:10.5281/zenodo.4548614.


## ACKNOWLEDGMENTS


We acknowledge G. Pooley's contribution to the radio observing campaign. The VLBA is a facility of the National Science Foundation operated under cooperative agreement by Associated Universities Inc. This work made use of the Swinburne University of Technology software correlator, developed as part of the Australian Major National Research Facilities Programme and operated under license. This work has made use of data from the European Space Agency (ESA) mission *Gaia* (www.cosmos.esa.int/gaia), processed by the *Gaia* Data Processing and Analysis Consortium (DPAC; www.cosmos.esa.int/web/gaia/dpac/consortium). Funding for the DPAC has been provided by national institutions, in particular the institutions participating in the *Gaia* Multilateral Agreement. **Funding:** J.C.A.M.-J. and I.M. are recipients of Australian Research Council Future Fellowships (FT140101082 and FT190100574, respectively) funded by the Australian government. L.G. acknowledges support from the National Program on Key Research and Development Project through grant 2016YFA0400804, and from the National NSFC with grant U1838114, and by the Strategic Priority Research Program of the Chinese Academy of Sciences through grant XDB23040100. V.G. is supported through the Margarete von Wrangell fellowship by the ESF and the Ministry of Science, Research and the Arts Baden-Württemberg. B.M. acknowledges support from the Spanish Ministerio de Economía y Competitividad (MINECO) under grant AYA2016-76012-C3-1-P and from the Spanish Ministerio de Ciencia e Innovación under grants PID2019-105510GB-C31 and CEX2019-000918-M of ICCUB (Unidad de Excelencia "María de Maeztu" 2020–2023). S.M. was supported by the Netherlands Organization for Scientific Research (NWO) VICI grant (639.043.513). G.R.S. acknowledges support from an NSERC Discovery Grant (RGPIN-2016-06569). V.T. is supported by program Laplas VI of the Romanian National Authority for Scientific Research. J.W. acknowledges funding from the Bundesministerium für Wirtschaft und Technologie under Deutsches Zentrum für Luft- und Raumfahrt grant 50 OR 1606. J.Z. acknowledges the support from the Polish National Science Centre grant 2015/18/A/ST9/00746. **Author contributions:** J.C.A.M.-J. analyzed the VLBA data and led the manuscript preparation. A.B. conducted the astrometric fitting. J.A.O. conducted the optical light curve and radial velocity curve fitting. I.M. and C.J.N. performed the stellar wind modeling and led the discussion of the system's evolution, with input from T.J.M.; L.G., X.Zha., and X.Zhe. performed the analysis of the black hole spin. J.Z. calculated the mass-luminosity tracks. M.J.Re. provided the archival VLBA data and guidance on precision astrometry. P.U., V.G., J.C.A.M.-J. and J.W. coordinated the VLBA observing campaign, with theoretical input from S.M.; J.C.A.M.-J., P.U., T.J.M., V.T., A.P.R., J.W., and D.M.R. wrote the observing proposal, and D.-Y.B., R.D., T.J., J.-S.K., B.M., M.J.Ri., G.R.S., and A.J.T. contributed to the design and setup of the observations. All authors provided input and comments on the manuscript. **Competing interests:** The authors declare no conflicts of interest. **Data and materials availability:** The raw VLBA data are available from the NRAO archive at https://archive.nrao.edu/archive/advquery.jsp under project codes BR141 and BM429. Our measured positions are listed in table S1. The COMPAS population synthesis code is available at http://github.com/TeamCOMPAS/COMPAS. Our software for performing the astrometric and optical model fitting, the spin fitting, and for calculating the mass-luminosity relationships, together with our COMPAS input and output files, are available at https://github.com/bersavosh/CygX-1_JMJ2021 and archived at https://zenodo.org/record/4548614 (*32*).


## SUPPLEMENTARY MATERIALS

science.sciencemag.org/content/371/6533/1046/suppl/DC1
Materials and Methods
Supplementary Text
Figs. S1 to S11
Tables S1 to S3
References (*33*–*118*)


18 February 2020; accepted 23 December 2020
Published online 18 February 2021
10.1126/science.abb3363

Science

# Cygnus X-1 contains a 21–solar mass black hole—Implications for massive star winds

James C. A. Miller-JonesArash BahramianJerome A. OroszIlya MandelLijun GouThomas J. MaccaroneCoenraad J. NeijsselXueshan ZhaoJanusz Zió#kowskiMark J. ReidPhil UttleyXueying ZhengDo-Young ByunRichard DodsonVictoria GrinbergTaehyun JungJeong-Sook KimBenito MarcoteSera MarkoffMaría J. RiojaAnthony P. RushtonDavid M. RussellGregory R. SivakoffAlexandra J. TetarenkoValeriu TudoseJoern Wilms

*Science*, 371 (6533), • DOI: 10.1126/science.abb3363

**A heavy black hole in an x-ray binary**

If a black hole interacts with a binary companion star, the system emits x-rays and can form a radio jet. The masses of black holes in these x-ray binaries are all lower than those detected using gravitational waves, challenging models of black hole formation from massive stars. Miller-Jones *et al.* used radio astrometry to refine the distance to Cygnus X-1, a well-studied x-ray binary. They found a larger distance than previous estimates, raising the mass of the black hole in the system to 21 solar masses. The results challenge the wind mass loss rates implemented in stellar evolution models.

*Science*, this issue p. 1046